

Article

Initial β Grain Size Effect on High-Temperature Flow Behavior of Tb8 Titanium Alloys in Single β Phase Field

Qiuyue Yang ¹, Min Ma ², Yuanbiao Tan ^{1,*}, Song Xiang ¹ , Fei Zhao ¹ and Yilong Liang ¹

¹ Guizhou Key Laboratory of Materials Mechanical Behavior and Microstructure, College of Materials and Metallurgy, Guizhou University, Guiyang 550025, China

² College of Materials Science and Engineering, Hunan University of Science and Technology, Xiangtan 411201, China

* Correspondence: ybtan1@gzu.edu.cn; Tel.: +86-147-85158006

Received: 25 June 2019; Accepted: 9 August 2019; Published: 15 August 2019



Abstract: The high-temperature flow behavior of TB8 titanium alloys with two different grain sizes was investigated in this present work. Results show that a significant characteristic of stress drop is visible at the start stage of the hot deformation process when the strain rates are 10^0 and 10^{-1} s^{-1} . With the further increasing of strain, the flow stress initially rises to a maximum value and subsequently attains a plateau for the strain rates of 10^0 s^{-1} and a slight decrease for the strain rates of 10^{-1} s^{-1} . Only dynamic recovery occurs under these deformation conditions. When the strain rates drop to 10^{-3} s^{-1} , the dynamic recrystallization takes place during hot deformation. The values of deformation activation energy and materials constants at different strains were calculated. The processing maps at different strains were established for the fine- and coarse-grained alloys. The optimal processing parameter for hot processing was attained to be $900 \text{ }^\circ\text{C}/10^{-3} \text{ s}^{-1}$ for fine-grained alloys and $950 \text{ }^\circ\text{C}/10^{-3} \text{ s}^{-1}$ for coarse-grained alloys, respectively.

Keywords: TB8 titanium alloy; hot deformation; flow behavior; dynamic recrystallization; microstructure

1. Introduction

Titanium alloys with metastable β phase structure exhibit an ultra-high strength, exceptional corrosion resistance, outstanding fracture toughness, and reasonable ductility, which has been extensively used as structural materials in the aerospace field [1–3]. TB8 titanium alloy is a new class of titanium alloys, recently developed from $\beta 21\text{s}$ alloy designed by the United States. The ultimate tensile strength of TB8 titanium alloy is higher than 1300 MPa after solution and aging treatment [4,5]. Therefore, the TB8 titanium alloy is widely used, instead of steel and TC4 alloy, to manufacture aircraft fasteners. Nevertheless, TB8 titanium alloy exhibits a larger deformation resistance and a narrow hot-working range during forging process. It is very hard to manufacture TB8 titanium alloy into a product with complicated shape by the means of hot rolling, hot forging, and hot extrusion in actual industrial processes [6,7]. It is well known that the mechanical properties of critical parts are significantly affected by the microstructure of TB8 titanium alloy formed during forging process. Thus, it is rather critical to better control the deformation microstructure for TB8 titanium alloy to achieve desired mechanical properties.

Generally, the flow behavior of metal materials during thermo-mechanical processing is remarkably affected by initial microstructure and other processing factors, including strain, strain rate, and deformation temperature [8–12]. Zhang et al. [11] reported that the initial morphology of α phase clearly affects the flow behavior of Ti-6Al-4V alloys under high deformation temperature. For the

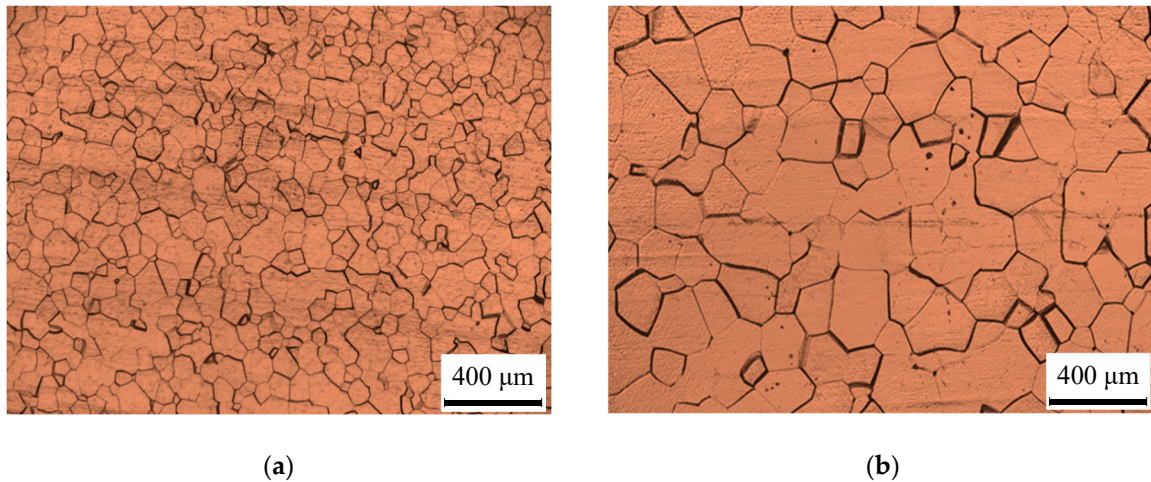
samples with a transformed β phase microstructure, the globularization of lamellar α phase was observed at strain rate lower than 10^{-3} s^{-1} during hot deformation in the $\alpha + \beta$ phase field, while the adiabatic shear band was formed at strain rate above 10^{-3} s^{-1} . For the samples containing a bimodal starting microstructure, an equiaxed grain microstructure was mainly presented at the condition of lower strain rates. In addition, the initial grain size of the β phase also has a distinct effect on the hot deformation behavior of metal materials [13–19]. Wahabi et al. [13] reported that dynamic recrystallization of the austenitic stainless steels with small initial grain sizes more easily occurred than that of coarse initial grain sizes at the same deformation condition. Ashtiani et al. [14] showed that the flow stress decreased with the rising of initial grain size at the strain rate of 0.5 s^{-1} , while increasing with the rising of initial grain size at strain rate lower than 0.05 s^{-1} in commercial pure aluminum. Barnett et al. [16,17] found that the peak stress was higher in Mg-3Al-1Zn alloys with coarse grain size than in that with fine grain size. Similar results were also observed in 7075 aluminum alloy [18] and 47Zr-45Ti-5Al-3V alloy [19]. Above all, the initial grain size presents different effects on the flow behavior of the metal materials owing to the difference in chemical compositions. In recent years, some studies have been performed to investigate the high-temperature flow behavior of TB8 titanium alloy under different deformation conditions in the $\alpha + \beta$ and single β phase field [20,21]. However, there have been few studies about the high-temperature flow behavior of TB8 titanium alloys containing different initial grain sizes. Thus, the objective of this present work was to thoroughly understand the effect of initial grain size on hot deformation behavior of TB8 titanium alloys based on the true stress-strain curve, processing maps for hot working, and microstructure analysis.

2. Experiments

The received TB8 titanium alloy is a forged bar with 60 mm in diameter. Table 1 lists the chemical composition of the alloy. The T_{β} temperatures of this alloy were measured to be $815 \text{ }^{\circ}\text{C}$ [21]. To investigate the initial grain size effect on the hot deformation behavior of TB8 titanium alloy in the single β phase field, the forged bar was firstly subjected to a solution treatment at 900 and 1000 $^{\circ}\text{C}$ for 0.5 h in a vacuum furnace which had been vacuumed and protected by argon gas, and the bars were subsequently placed in water for cooling. Figure 1 illustrates the initial microstructures of the heat-treated bars. The average grain sizes of the heat-treated bars were calculated by using the linear intercept method to be 87.43 μm and 184.25 μm , respectively. The compression samples with a height of 12 mm and a diameter of 8 mm were prepared from the bar that had been heat treated. These samples were subjected to the isothermal compression tests on a Gleeble 3500 thermal simulator (Dynamic Systems Inc. (DSI), Poestenkill, NY, USA). The range of deformation temperature was from 850 to 1000 $^{\circ}\text{C}$ with an interval of 50 $^{\circ}\text{C}$ and the range of strain rate was from 10^{-3} to 10^0 s^{-1} . The end surfaces of the cylindrical sample were smeared by the graphite lubricant, and tantalum foil was added between the sample and the punch to reduce the effect of deformed friction at the interface of punch and specimen during the hot deformation. The deformed samples were directly heated to a given deformation temperature at a rate of 20 $^{\circ}\text{C}/\text{s}$. In order to eliminate the thermal gradient of samples prior to deformation, they were soaked for 5 min at a given deformation temperature and then compressed to a true strain of 0.7 at a constant strain rate. The deformation temperature was monitored by a thermocouple welded at the mid-span of the samples. In order to maintain the deformed microstructure during hot deformation, the deformed samples were quickly cooled to room temperature with water sprays after deformation. To gain insight on the relationship between the microstructure evolutions of TB8 titanium alloy and hot processing parameters during hot deformation, all deformed samples were cut along the radial direction of the cylinder. Microstructure observation was performed on a Leica DMI5000M optical microscope (OM, Wetzlar, Germany). Samples for optical microscopy were mechanically polished and chemically etched using a solution of 10% HF, 30% HNO_3 , and 60% H_2O . Electron Backscattered Diffraction (EBSD) (Oxford Instruments, Abingdon, UK) technique was used to characterize the microstructure of deformed samples. The electrolyte consisting of 70% methanol, 20% ethylene glycol, and 10% perchloric acid was used to electronically polish EBSD samples.

Table 1. Chemical composition of the TB8 titanium alloys (Wt.%).

Mo	Al	Nb	Si	Fe	C	N	O	H	Ti
14.5	2.9	2.85	0.19	0.07	0.02	0.02	0.09	0.002	Bal

**Figure 1.** Microstructure of the TB8 titanium alloy after annealing at (a) 900 °C and (b) 1000 °C for 30 min.

3. Results and Discussion

3.1. Flow Curves

Figure 2 illustrates the flow curves of TB8 titanium alloys with two initial grain sizes at different deformation conditions. At the strain rate of 10^0 s^{-1} , the flow stress firstly rose to a maximum value with the rising of true strain, and then abruptly decreased to a lower value at all deformation temperatures for the samples with two different grain sizes, exhibiting a phenomenon of discontinuous stress drop after yielding (Figure 2a,e). The magnitude of the discontinuous stress drop was approximately 10–30 MPa and decreased with the rising of deformation temperature. A similar phenomenon has been found in other β titanium alloys [12,22]. The phenomenon of the discontinuous stress drop can be interpreted by the dynamic theory of discontinuous yielding [22]. The dynamic theory indicates that the mobile dislocations can be quickly generated from grain boundary sources during hot deformation, causing plastic deformation to move from the grain boundary to the interior of the grains. With further increasing of the strain, the flow stress slightly rises to a larger value. When the strain exceeds 0.2, the flow stress reaches a steady-state or slightly decreases, which is probably ascribed to adiabatic heating, flow instability, dynamic recovery, and dynamic recrystallization [23–25]. Further studies are need to verify these deformation mechanisms during hot deformation.

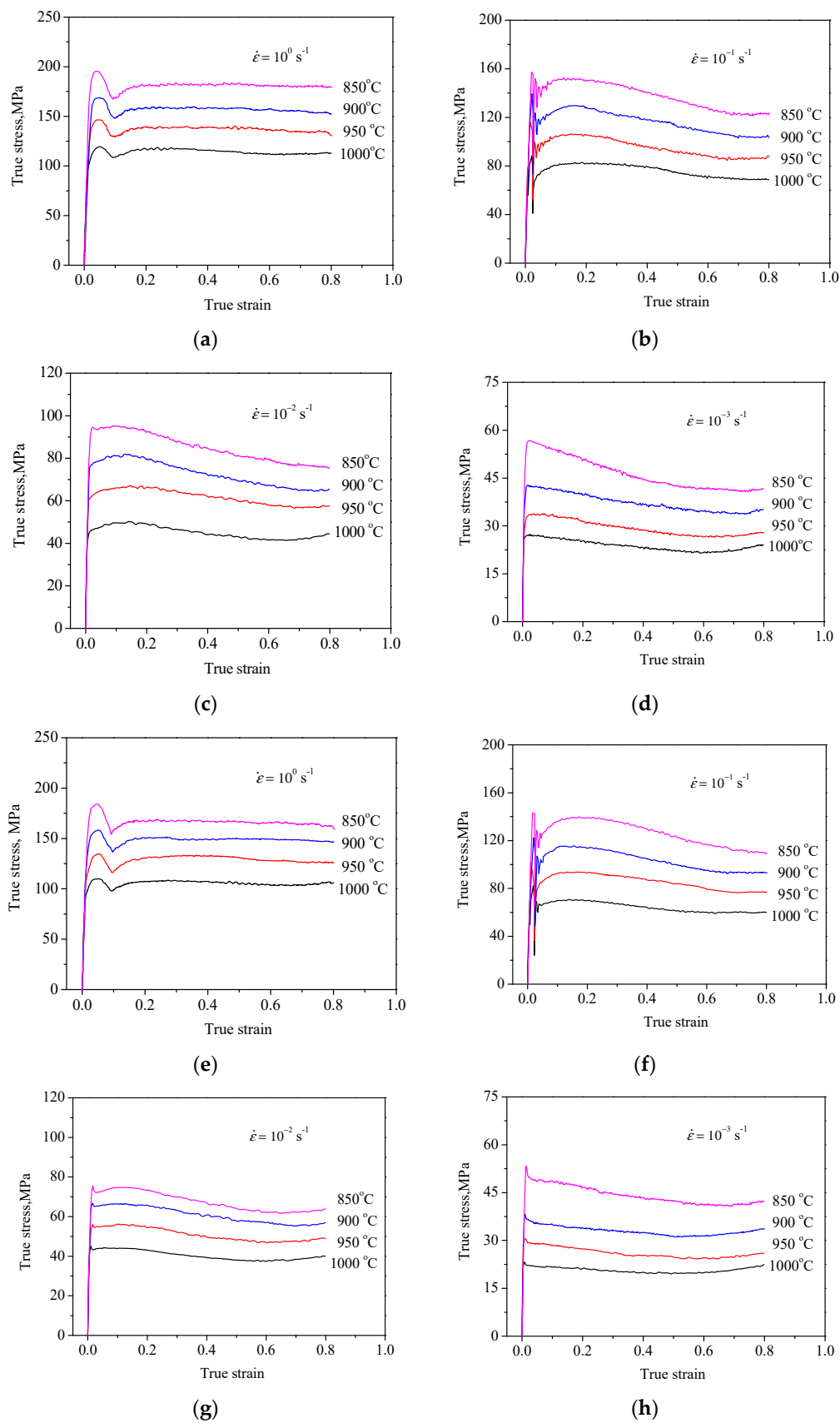


Figure 2. Stress-strain curves for the coarse-grained (a–d) and fine-grained (e–h) TB8 titanium alloys deformed at different strain rates.

When the strain rate was below 10^{-2} s^{-1} , the phenomenon of the discontinuous stress drop was gradually invisible for the alloys with two different grain sizes (Figure 2c–h). At a given deformation condition, it was noted that the significant discontinuous stress drop was lower for the TB8 titanium alloys with larger initial grain size, as shown in Figure 3. This is because the alloy with larger grain size owns only a few grain boundaries per unit volume, which reduces the grain boundary dislocation sources compared with the alloy with smaller grain size. It was interesting to note that a load drop and secondary yield point were visible on the flow curves of the initial deformation stage at the strain rate of 10^{-1} s^{-1} (Figure 2c,d). This phenomenon is also observed in Ti60 alloy [26] and superalloys [27,28], which could be caused by microstrain dynamic strain aging. Figure 2d,h shows that the flow curves with dynamic recrystallization characteristics were observed at the strain rate of 10^{-3} s^{-1} , indicating that the alloys with two different grain sizes had undergone dynamic recrystallization under these deformation conditions.

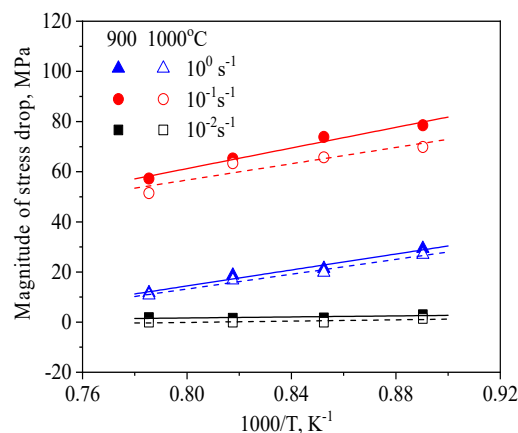


Figure 3. Magnitude of the stress drop as a function of deformation temperature and strain rate.

As noted previously, the deformation parameters and initial microstructure have significant effects on the hot deformation behavior of TB8 titanium alloy. However, it is difficult to accurately discover the deformation mechanism of TB8 titanium alloy by analyzing only the change in the shape of flow curves. This is because different microstructural evolution mechanisms may result from the same flow behavior during hot deformation. For example, both dynamic recovery and superplasticity can result in a steady flow stress in the late stage of hot deformation, while the flow softening in flow stress may be due to the globularization of lamellar α phase, adiabatic heating, or dynamic recrystallization [24,29,30]. Thus, the hot deformation behavior of the TB8 titanium alloy needs to be discussed in depth by the analysis of constitutive equations, processing maps, and deformation microstructure in order to accurately reveal the hot deformation mechanisms of the TB8 titanium alloy.

3.2. Constitutive Equations Analysis of TB8 Titanium Alloys

The process of hot deformation is mainly regulated by thermal-activation and strongly affected by the hot processing parameters, which has been illustrated by abundant literature on the hot deformation of different metal materials. Therefore, it is very significant to accurately describe the effect of processing parameters on flow behavior. The representative stress of each flow curve obtained from the maximum stress on each flow curve was selected. Figures 4 and 5 illustrate the relationship between the peak stress and hot processing parameters, respectively. It can be seen that an increasing trend was observed when deformation temperature decreased and strain rate increased for the TB8 titanium alloys containing different initial grain sizes. It is a remarkable fact that the values of peak stress were increased with the rising of grain size under the same deformation conditions, which is inverse to Hall–Petch relationship. A similar result is also found in commercially pure aluminum [14], Mg-3Al-1Zn [17], 7075 aluminum alloy [18], and AZ31 alloy [31]. This could result from the fact that the

deformation mechanism is mainly grain boundary sliding (GBS), instead of dislocation gliding, during hot deformation of TB8 titanium alloy [18,31,32]. For TB8 titanium alloy with coarse grain structure, there is a decreasing participation of GBS compared with TB8 titanium alloy with fine grain structure, which can effectively increase the flow stress during high-temperature deformation. Moreover, it is worth noting that TB8 titanium alloy with coarse grain structure owns only a few grain boundaries per unit volume, which reduces the number of the nucleation sites for dynamic recrystallization and is disadvantageous for the dynamic recrystallization of the alloys during hot deformation. Thus, the volume fraction of dynamic recrystallization for TB8 titanium alloy with coarse grain structure is less compared with TB8 titanium alloy with fine grain structure, which leads to an increase in flow stress.

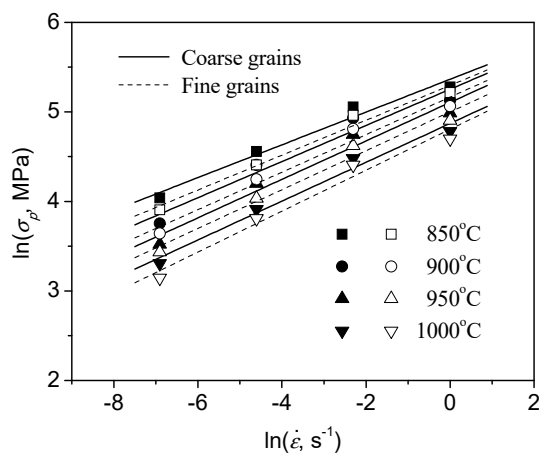


Figure 4. Relationship between the peak-stress and strain rate for the TB8 titanium alloys with two different initial grain sizes.

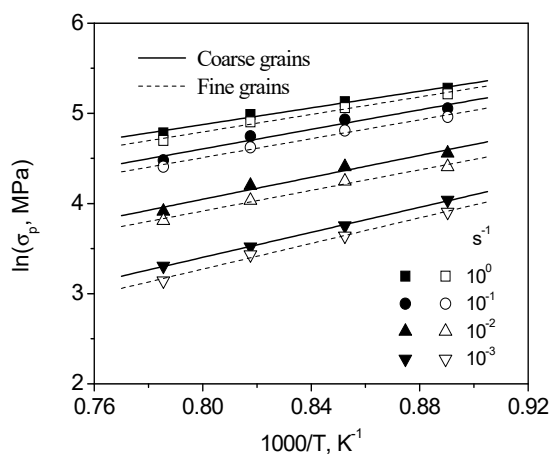


Figure 5. Relationship between the peak-stress and deformation temperature for the TB8 titanium alloys with two different initial grain sizes.

A hyperbolic-sine Arrhenius-type equation was proposed to describe the correlation between flow stress and hot processing parameters. The equation can be used to predict the constitutive behavior of most metals and alloys during hot deformation and can be mathematically expressed as [33]:

$$\dot{\epsilon} = A[\sinh(\alpha\sigma_p)]^n \exp(-Q/RT), \quad (1)$$

where σ_p stands for the peak stress (MPa). A (s^{-1}) and α (MPa^{-1}) are representative of materials constants. n and Q are representative of the stress exponent and the apparent activation energy for hot deformation ($J \cdot mol^{-1}$), respectively. The value of R is $8.314 J \cdot K^{-1} \cdot mol^{-1}$, $\dot{\epsilon}$ and T are the strain rate (s^{-1})

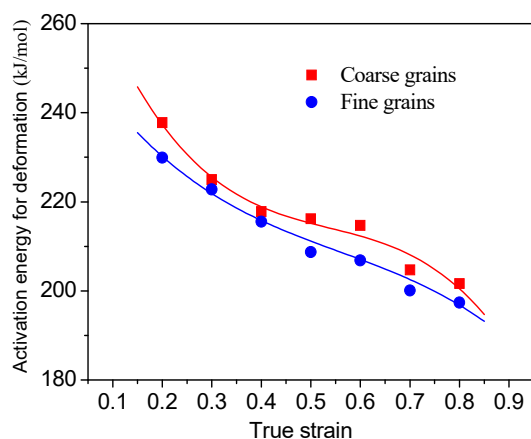


Figure 6. Variation of the activation energy of deformation (Q) with true strain for the TB8 titanium alloys with two different initial grain sizes.

The strain rate and deformation temperature are often incorporated to a single parameter, namely the Zener–Hollomon parameter ($Z = \dot{\epsilon} \exp(\frac{Q}{RT})$). According to the kinetic rate equation established by the obtained experimental data, the relationship between σ_p and Z can be characterized as shown in Figure 7. Obviously, the σ_p linearly rose with an increase in the value of Z , revealing that the constructed constitutive equation of hyperbolic sine function is effective for TB8 titanium alloys with two initial grain sizes during hot deformation.

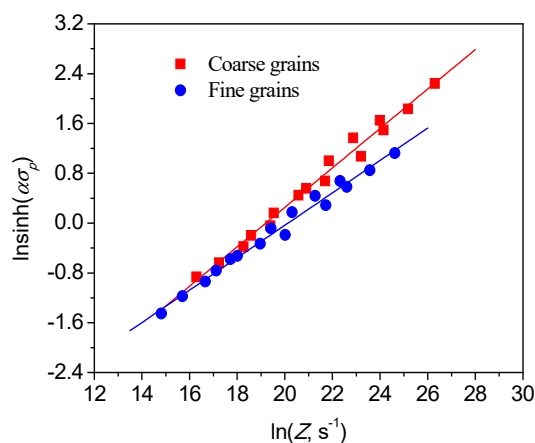


Figure 7. Variation in the peak stress (σ_p) with the Z parameter for the TB8 titanium alloys with two different initial grain sizes in the single β phase field.

The relationship between σ_p and Zener–Hollomon parameter can be described as:
 For TB8 titanium alloy with fine grain structure,

$$\sigma_p = \frac{1}{0.015} \ln\left\{\left(\frac{Z}{1.3 \times 10^8}\right)^{\frac{1}{3.20}} + \left[\left(\frac{Z}{1.3 \times 10^8}\right)^{\frac{2}{3.20}} + 1\right]^{\frac{1}{2}}\right\}, \tag{5}$$

$$Z = \dot{\epsilon} \exp\left(\frac{234720}{RT}\right). \tag{6}$$

For TB8 titanium alloy with coarse grain structure,

$$\sigma_p = \frac{1}{0.015} \ln\left\{\left(\frac{Z}{2.2 \times 10^8}\right)^{\frac{1}{3.16}} + \left[\left(\frac{Z}{2.2 \times 10^8}\right)^{\frac{2}{3.16}} + 1\right]^{\frac{1}{2}}\right\}, \tag{7}$$

$$Z = \dot{\epsilon} \exp\left(\frac{245560}{RT}\right). \quad (8)$$

3.3. Processing Maps

The processing map is an effective means to verify the hot deformation mechanisms and optimize hot process parameters, which was established according to the dynamic materials mode (DMM) put forward by Prasad [37–41]. The processing map consists of the superposition maps of a power dissipation map and an instability map. The power dissipation map was constructed according to the change in the power dissipation efficiency (η) with deformation temperature and strain rate, which can be calculated as follows:

$$\eta = \frac{J}{J_{\max}} = \frac{2m}{m+1}, \quad (9)$$

where m is representative of the strain rate sensitivity of flow stress. A domain presented in the maps directly corresponds to a specific microstructural mechanism, such as superplastic deformation and dynamic recrystallization. The domain with a high power dissipation efficiency can be considered as the optimum processing condition, which should be further supported by the microstructure of deformed samples. The instability map can be constituted by the change in a dimensionless instability parameter ($\xi(\dot{\epsilon})$) with deformation temperature and strain rate, which can be expressed as follows:

$$\xi(\dot{\epsilon}) = \frac{\partial \lg[m/(m+1)]}{\partial \lg \dot{\epsilon}} + m < 0. \quad (10)$$

The domain with a negative value of $\xi(\dot{\epsilon})$ is regarded as a flow instability, which may be attributed to adiabatic shear bands, cavitation, or flow localization. In this paper, the processing maps of TB8 titanium alloys with two initial grain sizes at various true strains were constructed based on DMM, as illustrated in Figure 8. In these maps, the instable regions were marked by the shaded areas, while the stable regions were characterized by white areas. The number illustrated in the contour is the η value.

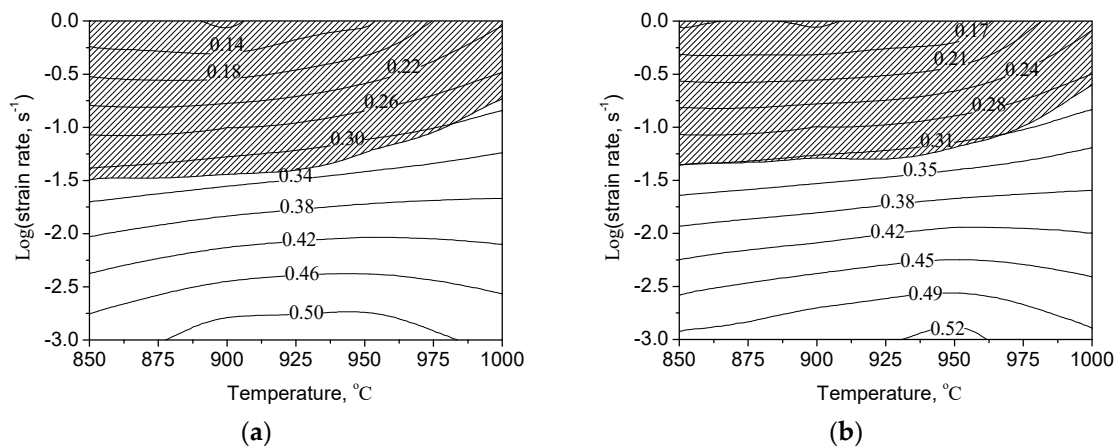


Figure 8. Cont.

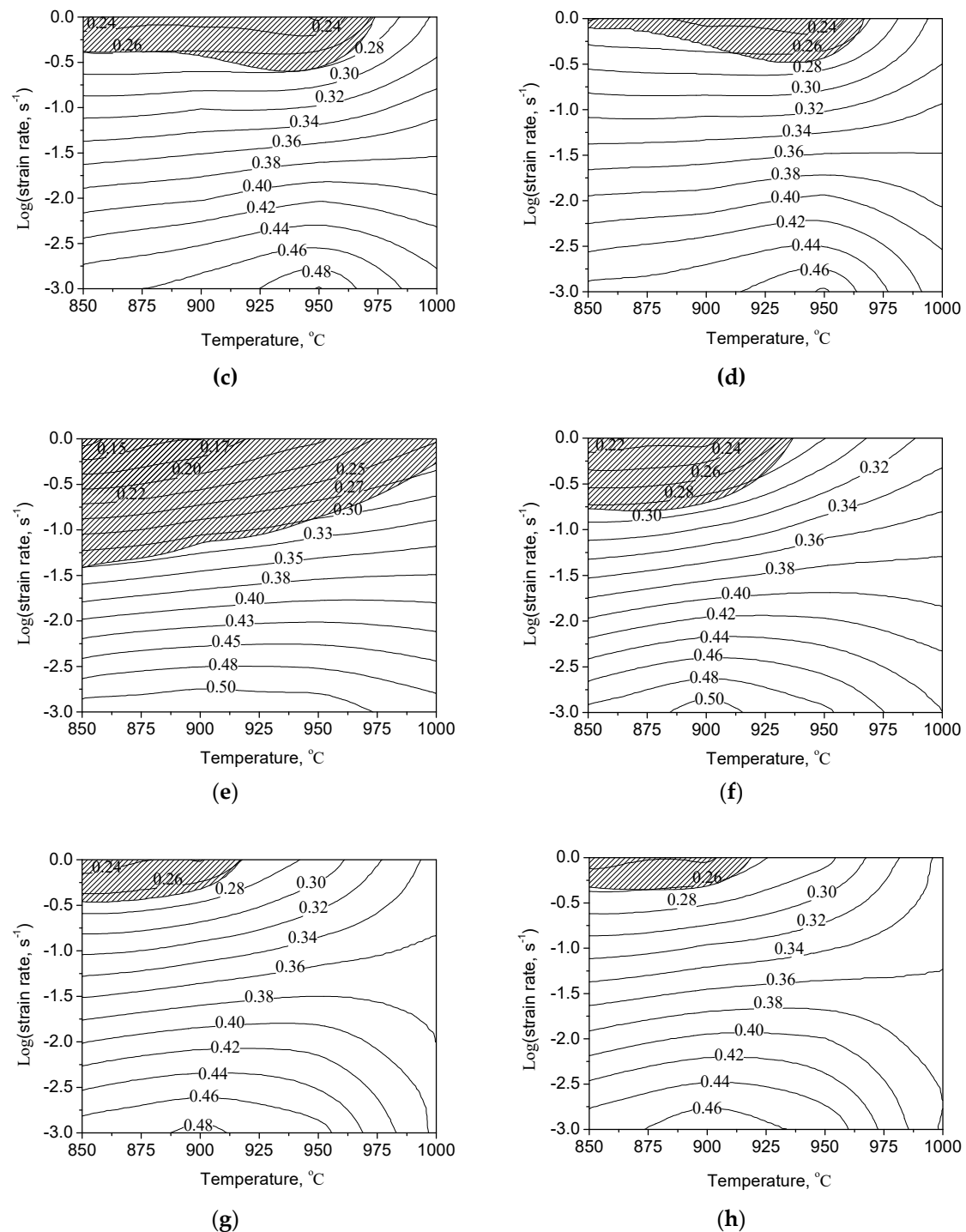


Figure 8. Processing maps of the coarse-grained (a–d) and fine-grained (e–h) alloys at true strains of (a,e) 0.2, (b,f) 0.5, (c,g) 0.7, and (d,h) 0.8.

At the strain of 0.2, it could be seen that a domain with a negative value of $\xi(\dot{\epsilon})$ was presented in the processing maps when the strain rate range is from 0.032 to 10^0 s^{-1} and the temperatures range is from 850 to 1000 °C for the TB8 titanium alloys with two initial grain sizes, as shown in Figure 8a,e. In general, the flow instability of the deformed samples during hot deformation is related to adiabatic shear bands at high strain rates [40–42]. The specific instability mechanisms should be verified by the microstructure observation of deformed samples in the instability regions. The region of flow instability gradually decreased when the true strain gradually rose (Figure 8b–h).

Moreover, at the strain of 0.2, the processing maps of the TB8 titanium alloys with two initial grain sizes all displayed a domain with the η value of approximate 0.50. It is interesting to note that the domain with a peak value of η presented in the temperature range of 880–985 °C and strain rate range of 1.91×10^{-3} – 10^{-3} s^{-1} for the TB8 titanium alloy with coarse-grained structure, whereas in the temperature range of 850–975 °C and strain rate range of $1.74 \cdot 10^{-3}$ – 10^{-3} s^{-1} for the TB8 titanium alloy with fine-grained structure. It is generally found that the power dissipation efficiency value of about 0.3–0.5 can be associated with dynamic recrystallization [43–45]. This suggests that the dynamic recrystallization has occurred at the strain of 0.2 for the TB8 titanium alloys with fine-grained and coarse-grained structure. Dynamic recrystallization was mainly the hot deformation mechanism of TB8 titanium alloy during hot deformation. To further analyze the microstructure characteristic of the TB8 titanium alloy deformed at the strain of 0.2, EBSD results of the TB8 titanium alloy with fine-grained sizes deformed at 900 °C/ 0.1 s^{-1} and true strain of 0.2 was observed, as illustrated in Figure 9. It can be seen from Figure 9a that the dynamic recrystallization only occurred in the local region of initial grain boundaries during hot deformation. In the EBSD maps, the black line and white line represented the high angle grain boundaries ($\theta > 15^\circ$, θ is the grain boundary orientation angle) and low angle grain boundaries ($2 < \theta < 15^\circ$), respectively. As was seen from Figure 9b, the volume fraction of low angle grain boundaries in Figure 8a accounts for 65.7%, suggesting that a large number of dislocations can be formed inside deformed grains when the alloy was deformed at the strain of 0.2. Figure 9c illustrates the local misorientation profile of the TB8 titanium alloy with fine-grained sizes along the gray line marked in Figure 9a. It is observed that only a small orientation gradient was observed in the interior of the grain, whereas the largest orientation gradient was located at the distance of approximate 5–10 μm from the grain boundaries and the misorientation angle is approximately 4–6°. This indicates that the deformation focuses mainly on the distance of approximate 5–10 μm from the grain boundaries at initial stage of hot deformation, and then proceeds into the interior of the grain. In general, grain boundary is considered as a strong obstacle to the dislocation slip from one crystal to its neighbor. However, it is interesting to note that the orientation gradient is almost unchanged near the grain boundaries, which can be attributed to that the mobile dislocation is absorbed by the grain boundaries. This is because that the grain boundaries may also act as dislocation sinks, notably during hot deformation.

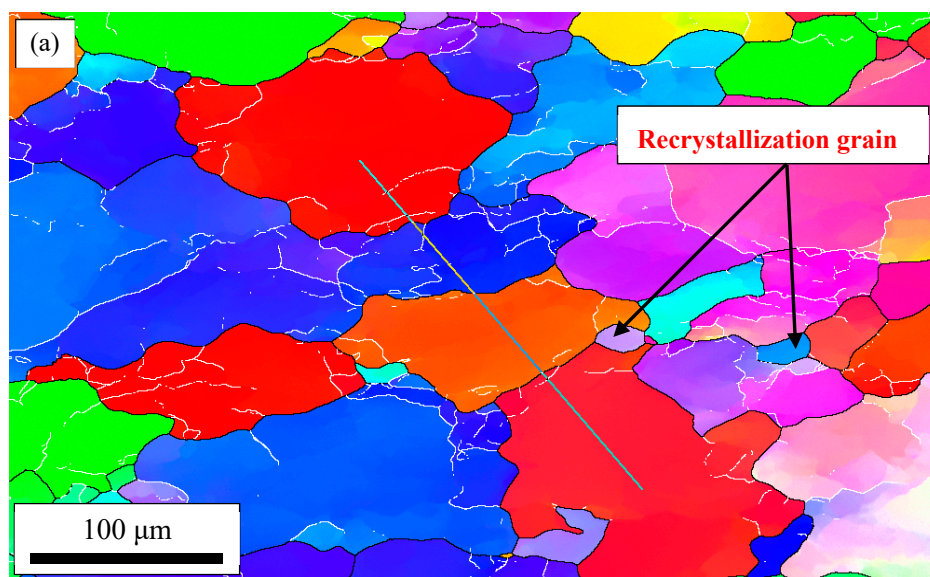


Figure 9. Cont.

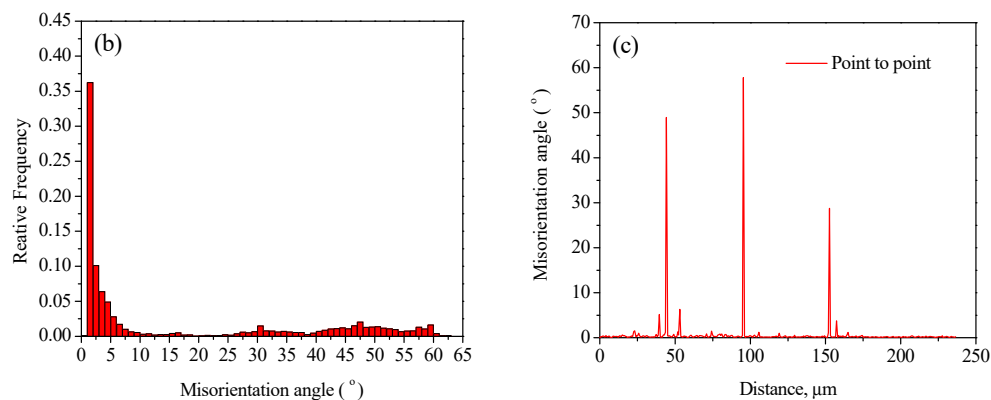


Figure 9. (a) Electron Backscattered Diffraction (EBSD) maps and (b) grain orientation profile of the TB8 titanium alloy with fine-grained sizes deformed at 900 °C, strain rate of 0.1 s⁻¹, and true strain of 0.2. (c) Local misorientation profile of the TB8 titanium alloy with fine-grained sizes along the gray line marked in (a). The compression axis is vertical.

When the true strain increases from 0.2 to 0.8, the locations of the domains with the peak power dissipation efficiency have no significant change for the TB8 titanium alloys with two initial grain sizes (Figure 8c–h). Thus, the domains with a peak value of η can be regarded as the optimal domain of hot working for TB8 titanium alloys with two initial grain sizes, respectively. By a comparison of the results obtained in Figure 8, it is noteworthy that the area of the flow instability of the fine-grained alloys is less than that of the coarse-grained alloys. Moreover, the deformation temperature corresponding to the domains with a peak value of η in the fine-grained alloys is lower than that in the coarse-grained alloys. This signifies that the TB8 titanium alloys with fine-grained structure are easily deformed, and the flow instability is not easily formed. It might be because the fine initial grains promote the dynamic recrystallization of the alloy during hot deformation.

For the sake of revealing the effect of deformation amount on the value of η during hot deformation of TB8 titanium alloys with two initial grain sizes, the relationship between the value of η and true strain is shown in Figure 10. It can be seen that the value of η raised firstly to a maximum value when the strain raised from 0.2 to 0.3. This may be attributed to the fact that the increase in strain energy with the rising of strain promotes the degree of the dynamic recrystallization of the TB8 titanium alloys. When the strain is higher than 0.3, the value of η presents a decreasing trend. Similar results were also observed in the Inconel 718 superalloy [46]. This is ascribed to the coarsening of the recrystallized grains [46]. Figure 11 exhibits the change in the microstructures of the fine-grained alloys deformed at 900 °C/10⁻³ s⁻¹ with true strain. It is observed that only a few fine recrystallized grains were illustrated in initial grain boundaries at the strain of 0.2 (Figure 11a). The number and size of recrystallized grains increased with the rising of strain (Figure 11b,c). The full dynamic recrystallization was obtained when the alloy was deformed at the strain of 0.8 (Figure 11d). It is noted that the value of η of the fine-grained alloys and coarse-grained alloys was higher than 0.48 in the strain range of 0.1 to 0.8. Thus, it is considered that 900 °C/10⁻³ s⁻¹ and 950 °C/10⁻³ s⁻¹ are the optimum processing parameters of the fine- and coarse-grained alloys for hot working, respectively. The dynamic recrystallization is mainly the hot deformation mechanism during the hot deformation of the TB8 titanium alloys with two initial grain sizes.

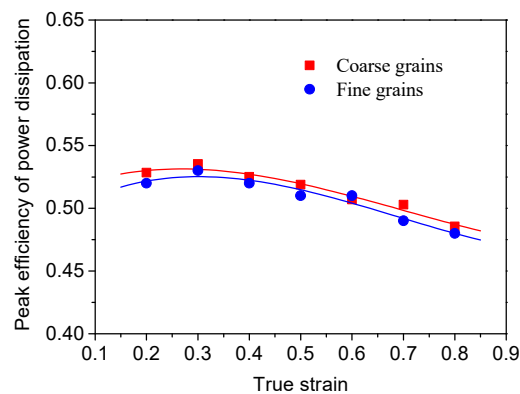


Figure 10. Variation in the efficiency of power dissipation with true strain at $950\text{ }^{\circ}\text{C}/10^{-3}\text{ s}^{-1}$ for the TB8 titanium alloy with coarse-grained sizes and $900\text{ }^{\circ}\text{C}/10^{-3}\text{ s}^{-1}$ for the TB8 titanium alloy with fine-grained sizes.

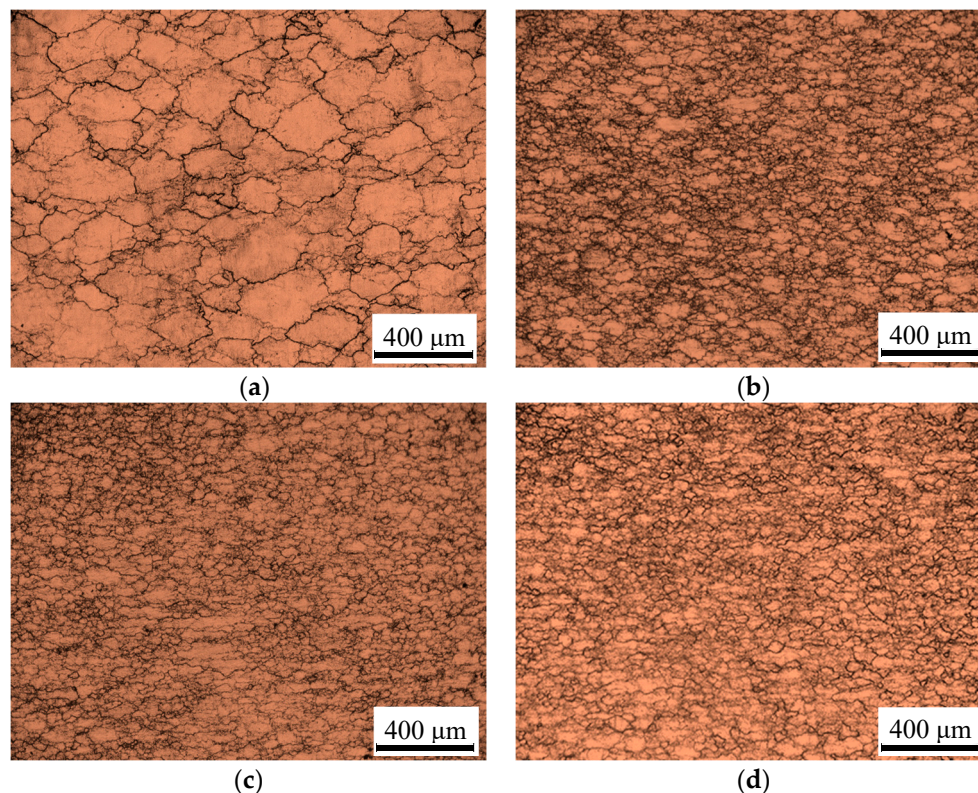


Figure 11. Optical microstructures of the fine-grained alloys deformed at $900\text{ }^{\circ}\text{C}/10^{-3}\text{ s}^{-1}$ and different true strains of (a) 0.2, (b) 0.4, (c) 0.6, and (d) 0.8.

3.4. Deformation Microstructure of TB8 Titanium Alloys

Many studies have reported that the cracking, flow localization, and dynamic strain aging could result in the flow instability during the hot deformation of the alloys, whereas dynamic recovery, dynamic recrystallization, or superplasticity could lead to a domain with the peak value of η in the processing maps [24,44–47]. To further analyze the specific mechanism in each region during hot deformation of the TB8 titanium alloys with two initial grain sizes, the typical microstructures of the TB8 titanium alloys with two initial grain sizes were observed, as shown in Figures 12 and 13. Obviously, the initial grains were only elongated along the radial, indicating that only dynamic recovery took place for the TB8 titanium alloys with two initial grain sizes (Figure 12a,d). Moreover,

a distinct phenomenon of flow localization was observed at $850\text{ }^{\circ}\text{C}/10^0\text{ s}^{-1}$. A similar phenomenon was also found in Ti-22Al-25Nb alloy [24] and TC21 alloys [8]. Generally, it is very easy to form the flow localization phenomenon when titanium alloys were deformed at the low temperatures and high strain rates in the single β phase field, which is attributed to the generation of deformation heating during hot working of titanium alloys [24]. When the strain rate gradually decreased and the deformation temperature gradually raised, the region of deformation gradually enlarges (Figure 12b,c,e,f). This is because low strain rates and high deformation temperature facilitate the release of the heat produced from the plastic deformation, restraining the formation of flow localization phenomenon.

Figure 13 illustrates typical microstructures of the TB8 titanium alloys with two initial grain sizes under different conditions in the stability region. For the TB8 titanium alloy with coarse-grained structure, only a small amount of recrystallized grains exist in the initial grain boundaries of deformed grains (Figure 13a). The number and size of recrystallized grains increased as the deformation temperature increased, (Figure 13b). When the deformation temperature raised to $950\text{ }^{\circ}\text{C}$ and the strain rate dropped to 10^{-3} s^{-1} , the full dynamic recrystallization occurs (Figure 13c), indicating that the dynamic recrystallization is mainly the hot deformation mechanism in the domain with a peak value of η . Li et al. [48] and Lu et al. [49] also reported that the highest value of η is generally obtained in the domains where dynamic recrystallization occurred. Hence, the domain with the highest value of η is considered as a favorable process window during hot deformation. As the deformation temperature is further raised, the recrystallized grains gradually coarsen. (Figure 13d). For the TB8 titanium alloys with fine-grained structure, it is observed from Figure 13e that plenty of fine recrystallized grains are formed in the initial grain boundary of deformed grains, suggesting that only partial recrystallization occurs under this deformation condition. Figure 13f shows that a full dynamic recrystallization occurred at $900\text{ }^{\circ}\text{C}/10^{-3}\text{ s}^{-1}$. When the deformation temperature raised from 900 to $1000\text{ }^{\circ}\text{C}$, the size of recrystallized grains gradually increased (Figure 13g,h). It is remarkable fact that at deformation temperature lower than $950\text{ }^{\circ}\text{C}$, the volume fraction of recrystallized grains for the coarse-grained alloys is lower than that for the fine-grained alloys under the same deformation condition. This is attributed to an increase in the number of grain boundaries per unit volume for the fine-grained alloys compared with the coarse-grained alloys, which results in a faster dynamic recrystallization under the same deformation. When the deformation temperature exceeded than $950\text{ }^{\circ}\text{C}$, the size of recrystallized grains all coarsen for TB8 titanium alloys with two initial grain sizes. The coarsening of grains was detrimental to the mechanical properties and processability of the materials and should also be avoided in the hot processing of TB8 titanium alloys.

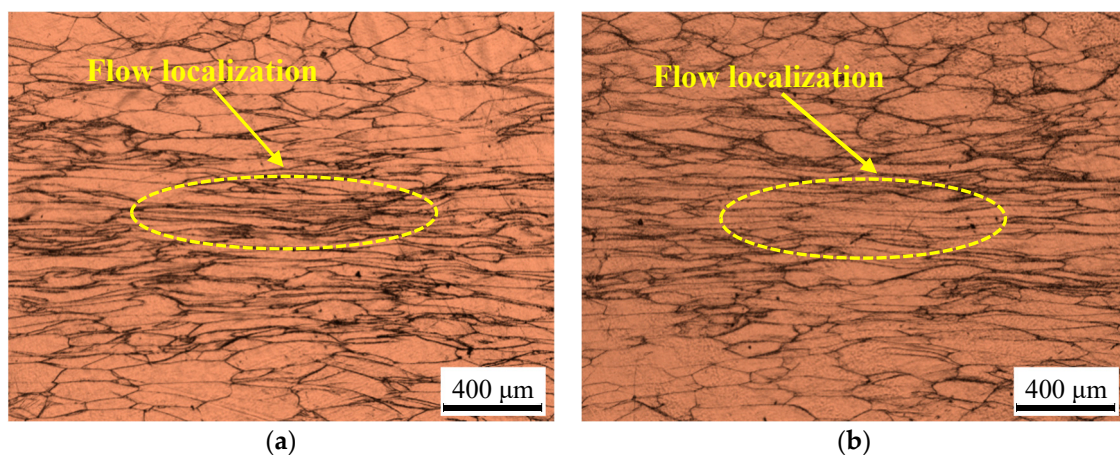


Figure 12. Cont.

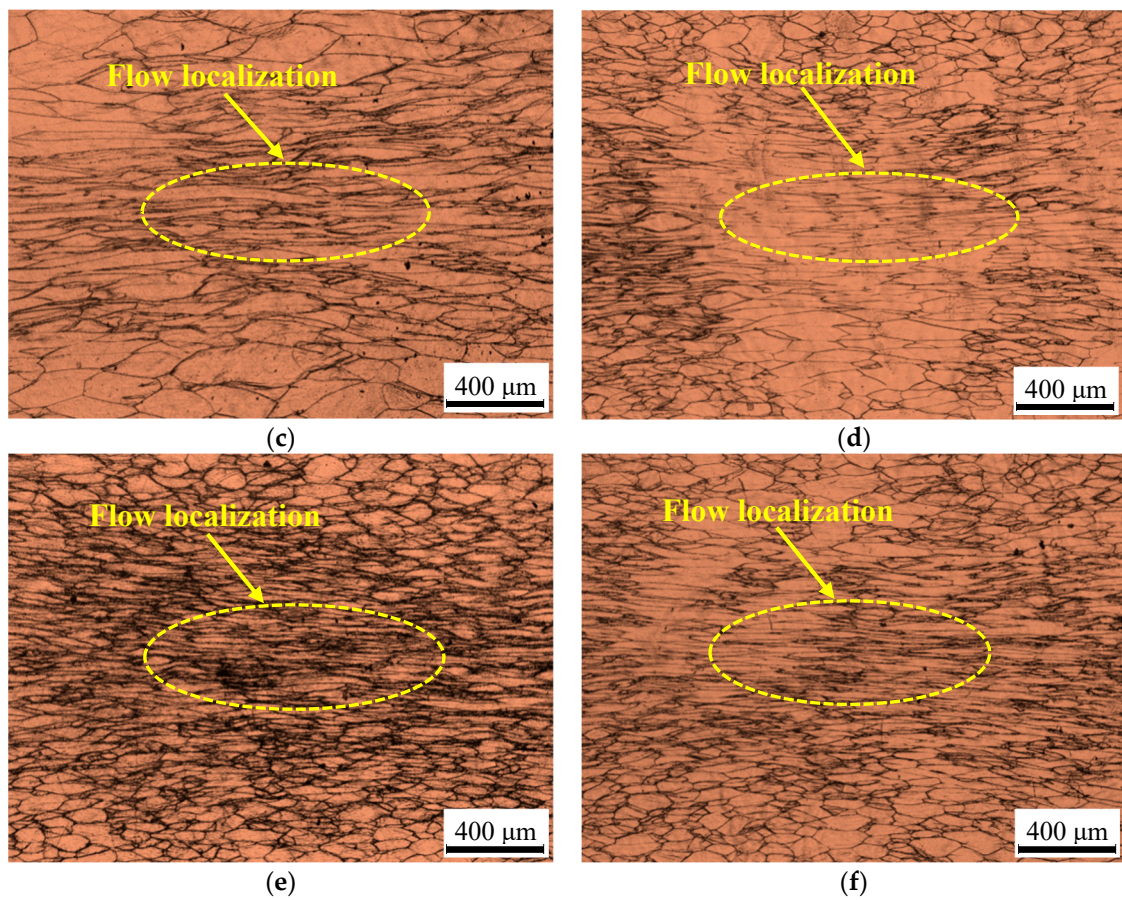


Figure 12. Optical microstructures of the coarse-grained (a–c) and fine-grained (d–f) alloys in the flow instability region at a strain of 0.8 and deformation conditions of (a,d) 850 °C/10⁰ s⁻¹, (b,e) 850 °C/10⁻¹ s⁻¹, and (c,f) 900 °C/10⁰ s⁻¹.

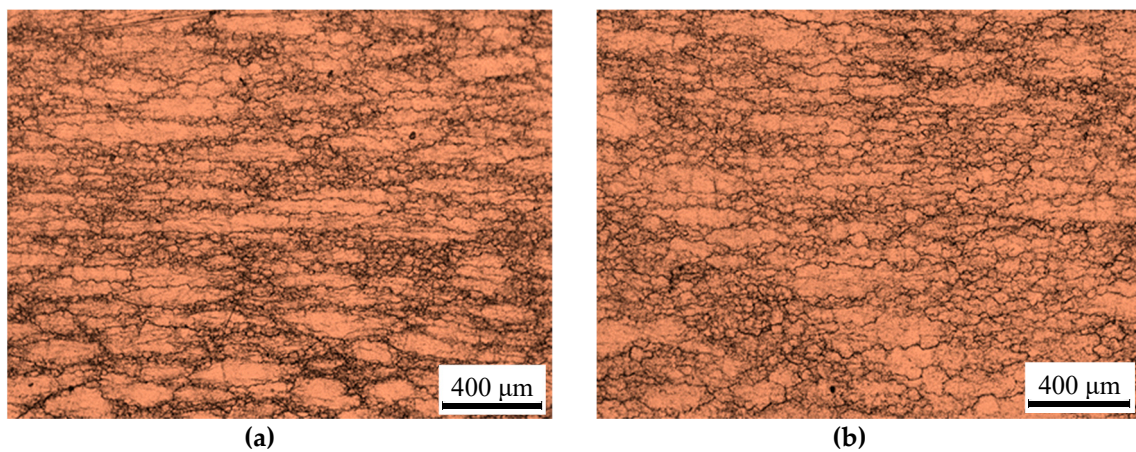


Figure 13. Cont.

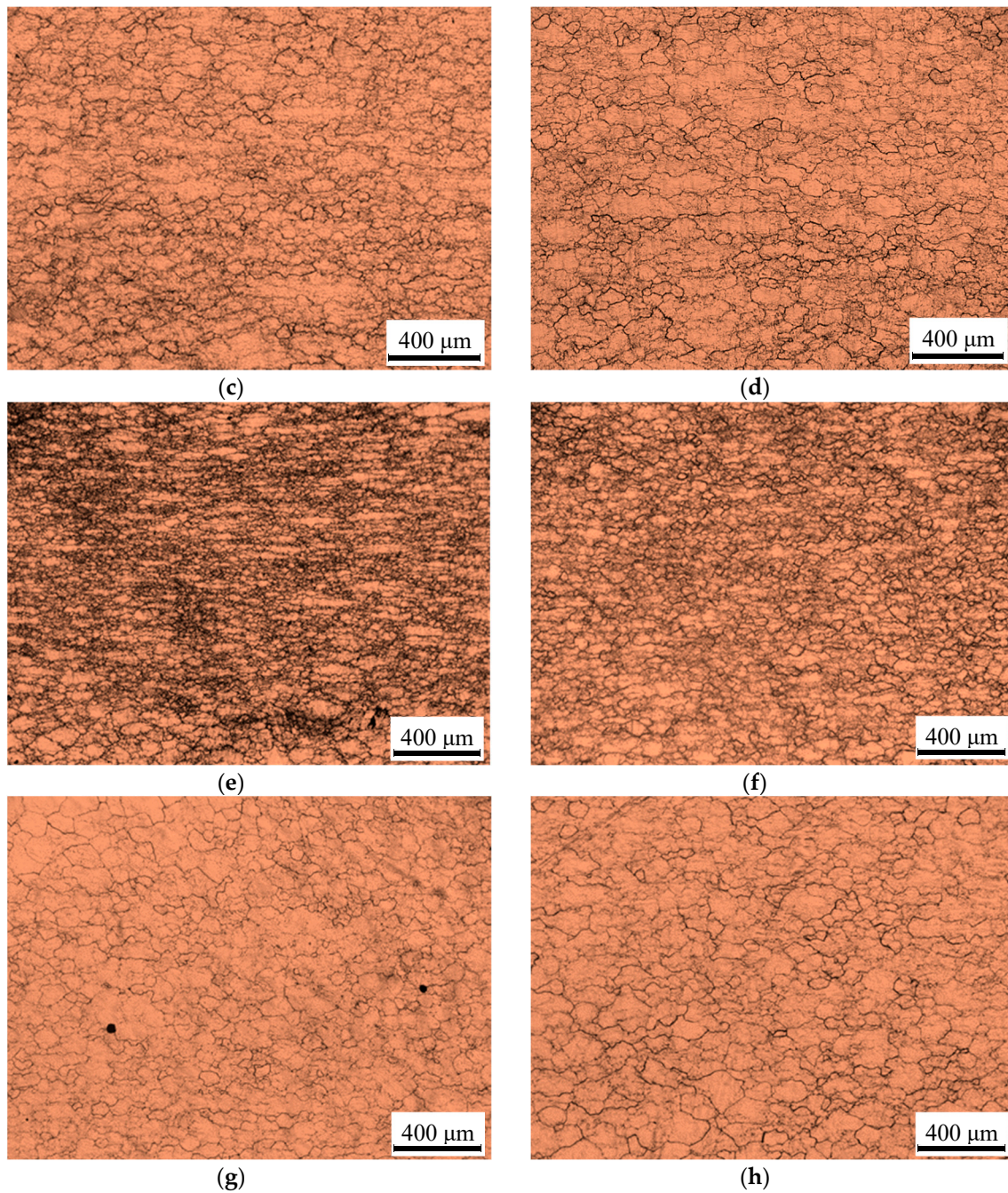


Figure 13. Optical microstructures of the coarse-grained (a–d) and fine-grained (e–h) alloys in the stability region at a strain of 0.8 and deformation conditions of (a,e) $850\text{ }^{\circ}\text{C}/10^{-3}\text{ s}^{-1}$, (b,f) $900\text{ }^{\circ}\text{C}/10^{-3}\text{ s}^{-1}$, (c,g) $950\text{ }^{\circ}\text{C}/10^{-3}\text{ s}^{-1}$, and (d,h) $1000\text{ }^{\circ}\text{C}/10^{-3}\text{ s}^{-1}$.

4. Conclusions

In this present work, initial β grain size effect on high-temperature flow behavior of TB8 titanium alloys with two different grain sizes in single β phase field was investigated. The main conclusions are presented as follows:

1. At the strain rates of 10^0 and 10^{-1} s^{-1} , a significant phenomenon of stress drop was visible at the beginning stage of deformation for TB8 titanium alloys with fine-grained and coarse-grained structure. The flow stress firstly raised to a maximum value, and subsequently attained a plateau at 10^0 s^{-1} , whereas a slight decrease at 10^{-1} s^{-1} . Only dynamic recovery occurs under these

deformation conditions. When the strain rate is 10^{-3} s^{-1} , the flow curves of TB8 titanium alloys showed a typical characteristic of dynamic recrystallization.

- The values of α , A , n , and Q were computed at various strains, according to the received experimental data for TB8 titanium alloys with two different grain sizes. The value of Q all declined gradually with the rising of strain. At a given strain, the value of Q for the fine-grained alloy is lower than that for the coarse-grained alloy, which indicates that the fine initial grain size is beneficial to the plastic deformation of the alloy during hot processing.
- The relationship between σ_p , $\dot{\epsilon}$ and T can be described by the hyperbolic-sine Arrhenius-type equation as follows: For TB8 titanium alloy with fine grain structure,

$$\dot{\epsilon} = 1.30 \times 10^8 [\sinh(\alpha\sigma_p)]^{3.20} \exp\left(-\frac{234720}{RT}\right). \quad (11)$$

For TB8 titanium alloy with coarse grain structure,

$$\dot{\epsilon} = 2.20 \times 10^8 [\sinh(\alpha\sigma_p)]^{3.16} \exp\left(-\frac{245560}{RT}\right). \quad (12)$$

- At the strain of 0.2, the dynamic recrystallization only occurred in the local region of initial grain boundaries during hot deformation for the TB8 titanium alloy with fine-grained structure. The volume fraction of low angle grain boundaries was accounted for 65.7%. The largest orientation gradient was located at the distance of approximate 5–10 μm from the grain boundaries and the misorientation angle was approximately $4\text{--}6^\circ$.
- The processing maps of TB8 titanium alloys with two different grain sizes were established. The optimum processing parameters of the fine- and coarse-grained alloy for hot working were measured to be $900 \text{ }^\circ\text{C}/10^{-3} \text{ s}^{-1}$ and $950 \text{ }^\circ\text{C}/10^{-3} \text{ s}^{-1}$, respectively. The hot deformation mechanism in these regions with a peak value of η is mainly the dynamic recrystallization of β phase.

Author Contributions: Methodology, S.X.; Software, F.Z.; Validation, Y.T.; Formal Analysis, M.M.; Writing—Original Draft Preparation, Q.Y.; Visualization, Y.L.

Funding: This work was supported by the National Natural Science Foundation of China (Grant no. 51804087 and 51661006), Science and Technology Cooperative Foundation of Guizhou province (Grant no. [2017]7240 and [2017]5788), Basic research program of Guizhou Province (Grant no. [2019]1091) and the innovative talents teams project of Guizhou Province (Grant no. 20175656).

Conflicts of Interest: The authors declare no conflict of interest.

References

- Boyer, R.R.; Briggs, R.D. The use of β titanium alloys in the aerospace industry. *J. Mater. Eng. Perform.* **2005**, *14*, 681–685. [[CrossRef](#)]
- Balasubrahmanyam, V.V.; Prasad, Y.V.R.K. Deformation behaviour of beta titanium alloy Ti-10V-4.5Fe-1.5Al in hot upset forging. *Mater. Sci. Eng. A* **2002**, *336*, 150–158. [[CrossRef](#)]
- Li, Y.H.Z.; Ou, X.Q.; Ni, S.; Song, M. Deformation behaviors of a hot rolled near- β Ti-5Al-5Mo-5V-1Cr-1Fe alloy. *Mater. Sci. Eng. A* **2019**, *742*, 390–399. [[CrossRef](#)]
- Xu, T.W.; Li, J.S.; Zhang, F.S.; Wang, F.Y.; Liu, X.H.; Feng, Y. Microstructure Evolution during Cold-Deformation and Aging Response after Annealing of TB8 Titanium Alloy. *Rare Met. Mater. Eng.* **2016**, *45*, 575–580. [[CrossRef](#)]
- Tang, B.; Tang, B.; Han, F.B.; Yang, G.J.; Li, J.S. Microstructure Evolution during Cold-Deformation and Aging Response after Annealing of TB8 Titanium Alloy. *J. Alloy. Compd.* **2013**, *565*, 1–5.
- Baufeld, B.; Biest, O.V.D.; Gault, R. Mechanical properties of Ti-6Al-4V specimens produced by shaped metal deposition. *Sci. Technol. Adv. Mater.* **2009**, *10*, 1–10. [[CrossRef](#)] [[PubMed](#)]
- Baufeld, B.; Biest, O.V.D.; Gault, R. Additive manufacturing of Ti-6Al-4V components by shaped metal deposition: Microstructure and mechanical properties. *Mater. Des.* **2010**, *31*, 106–111. [[CrossRef](#)]

8. Zhu, Y.C.; Zeng, W.D.; Liu, J.L.; Zhao, Y.Q.; Zhou, Y.G.; Yu, H.Q. Effect of processing parameters on the hot deformation behavior of as-cast TC21 titanium alloy. *Mater. Des.* **2012**, *33*, 264–272. [[CrossRef](#)]
9. Peng, W.W.; Zeng, W.D.; Wang, Q.J.; Zhao, Q.Y.; Yu, H.Q. Effect of processing parameters on hot deformation behavior and microstructural evolution during hot compression of as-cast Ti60 titanium alloy. *Mater. Sci. Eng. A* **2014**, *593*, 16–23. [[CrossRef](#)]
10. Liu, Y.H.; Ning, Y.Q.; Yao, Z.K.; Guo, H.Z. Hot deformation behavior of Ti-6.0Al-7.0Nb biomedical alloy by using processing map. *J. Alloy. Compd.* **2014**, *587*, 183–189. [[CrossRef](#)]
11. Zhang, Z.X.; Qu, S.J.; Feng, A.H.; Shen, J.; Chen, D.L. Hot deformation behavior of Ti-6Al-4V alloy: Effect of initial microstructure. *J. Alloy. Compd.* **2017**, *718*, 170–181. [[CrossRef](#)]
12. Long, S.; Xia, Y.F.; Hu, J.C.; Zhang, J.S.; Zhou, J.; Zhang, P.; Cui, M.L. Hot deformation behavior and microstructure evolution of Ti-6Cr-5Mo-5V-4Al alloy during hot compression. *Vacuum* **2019**, *160*, 171–180. [[CrossRef](#)]
13. El Wahabi, M.; Gavard, L.; Montheillet, F.; Cabrera, J.M.; Prado, J.M. Effect of initial grain size on dynamic recrystallization in high purity austenitic stainless steels. *Acta Mater.* **2005**, *53*, 4605–4612. [[CrossRef](#)]
14. Rezaei Ashtiani, H.R.; Parsa, M.H.; Bisadi, H. Effects of initial grain size on hot deformation behavior of commercial pure aluminum. *Mater. Des.* **2012**, *42*, 478–485. [[CrossRef](#)]
15. Oudin, A.; Barnett, M.R.; Hodgson, P.D. Grain size effect on the warm deformation behaviour of a Ti-IF steel. *Mater. Sci. Eng. A* **2004**, *367*, 282–294. [[CrossRef](#)]
16. Barnett, M.R.; Beer, A.G.; Atwell, D.; Oudin, A. Influence of grain size on hot working stresses and microstructures in Mg-3Al-1Zn. *Scr. Mater.* **2004**, *51*, 19–24. [[CrossRef](#)]
17. Barnett, M.R.; Keshavarz, Z.; Beer, A.G.; Atwell, D. Influence of grain size on the compressive deformation of wrought Mg-3Al-1Zn. *Acta Mater.* **2004**, *52*, 5093–5103. [[CrossRef](#)]
18. Yang, Y.B.; Zhang, Z.M.; Li, X.B.; Wang, Q.; Zhang, Y.H. The effects of grain size on the hot deformation and processing map for 7075 aluminum alloy. *Mater. Des.* **2013**, *51*, 592–597. [[CrossRef](#)]
19. Tan, Y.B.; Yang, L.H.; Duan, J.L.; Liu, W.C.; Zhang, J.W.; Liu, R.P. Effect of initial grain size on the hot deformation behavior of 47Zr-45Ti-5Al-3V alloy. *J. Nucl. Mater.* **2014**, *454*, 413–420. [[CrossRef](#)]
20. Duan, Y.P.; Ping, L.I.; Xue, K.M.; Zhang, Q.; Wang, X.X. Flow behavior and microstructure evolution of TB8 alloy during hot deformation process. *Trans. Nonferrous Met. Soc. China* **2007**, *17*, 1199–1204. [[CrossRef](#)]
21. Tang, B.; Tang, B.; Han, F.B.; Li, J.S.; Yang, G.J. Hot Deformation Behavior of TB8 Alloy near the β -Transus. *Rare Met. Mat. Eng.* **2013**, *42*, 1761–1766.
22. Philippart, I.; Rack, H.J. High temperature dynamic yielding in metastable Ti-6.8Mo- 4.5Fe-1.5Al alloy. *Mater. Sci. Eng. A* **1998**, *243*, 196–200. [[CrossRef](#)]
23. Semiatin, S.L.; Seetharaman, V.; Weiss, I. Flow behavior and globularization kinetics during hot working of Ti-6Al-4V with a colony alpha microstructure. *Mater. Sci. Eng. A* **1999**, *263*, 257–271. [[CrossRef](#)]
24. Ma, X.; Zeng, W.D.; Xu, B.; Sun, Y.; Xue, C.; Han, Y.F. Characterization of the hot deformation behavior of a Ti-22Al-25Nb alloy using processing maps based on the Murty criterion. *Intermetallics* **2012**, *20*, 1–7. [[CrossRef](#)]
25. Park, C.H.; Kim, J.H.; Hyun, Y.T.; Yeom, J.T.; Reddy, N.S. The origins of flow softening during high-temperature deformation of a Ti-6Al-4V alloy with a lamellar microstructure. *J. Alloy. Compd.* **2014**, *582*, 126–129. [[CrossRef](#)]
26. Peng, W.W.; Zeng, W.D.; Wang, Q.J.; Yu, H.Q. Characterization of high-temperature deformation behavior of as-cast Ti60 titanium alloy using processing map. *Mater. Sci. Eng. A* **2013**, *571*, 116–122. [[CrossRef](#)]
27. Yuan, H.; Liu, W.C. Effect of the δ phase on the hot deformation behavior of Inconel 718. *Mater. Sci. Eng. A* **2005**, *408*, 281–289. [[CrossRef](#)]
28. Coryell, S.P.; Findley, K.O.; Mataya, M.C. Evolution of Microstructure and Texture During Hot Compression of a Ni-Fe-Cr Superalloy. *Metall. Mater. Trans. A* **2012**, *43*, 633–649. [[CrossRef](#)]
29. Narayana Murty, S.V.S.; Nageswara Rao, B. On the flow localization concepts in the processing maps of titanium alloy Ti-24Al-20Nb. *J. Mater. Process. Technol.* **2000**, *104*, 103–109. [[CrossRef](#)]
30. Prasad, Y.V.R.K.; Seshacharyulu, T.; Medeiros, S.C.; Frazier, W.G. Influence of oxygen content on the forging response of equiaxed ($\alpha + \beta$) preform of Ti-6Al-4V: Commercial vs. ELI grade. *J. Mater. Process. Technol.* **2001**, *108*, 320–327. [[CrossRef](#)]
31. Atwell, D.L.; Barnett, M.R.; Hutchinson, W.B. The effect of initial grain size and temperature on the tensile properties of magnesium alloy AZ31 sheet. *Mater. Sci. Eng. A* **2012**, *549*, 1–6. [[CrossRef](#)]

32. Verlinden, B.; Driver, J.; Samajdar, I.; Doherty, D. *Thermo-Mechanical Processing of Metallic Materials*; Elsevier: Amsterdam, The Netherlands, 2007.
33. Sellars, C.M.; Tegart, W.J.M. Relationship between strength and structure in deformation at elevated temperatures. *Mem. Sci. Rev. Metall.* **1966**, *63*, 731–746.
34. Cai, J.; Li, F.G.; Liu, T.Y.; Chen, B.; He, M. Constitutive equations for elevated temperature flow stress of Ti-6Al-4V alloy considering the effect of strain. *Mater. Des.* **2011**, *32*, 1144–1151. [[CrossRef](#)]
35. Radovi, N.; Drobnjak, D. Effect of Interpass Time and Cooling Rate on Apparent Activation Energy for Hot Working and Critical Recrystallization Temperature of Nb-microalloyed Steel. *ISIJ Int.* **1999**, *39*, 575–582. [[CrossRef](#)]
36. Lee, W.S.; Lin, M.T. The effects of strain rate and temperature on the compressive deformation behaviour of Ti-6Al-4V alloy. *J. Mater. Process Technol.* **1997**, *71*, 235–246. [[CrossRef](#)]
37. Weissa, I.; Semiatin, S.L. Thermomechanical processing of beta titanium alloys-an overview. *Mater. Sci. Eng. A* **1998**, *243*, 46–65. [[CrossRef](#)]
38. Prasad, Y.V.R.K.; Gegel, H.L.; Doraivelu, S.M.; Malas, J.C.; Morgan, J.T.; Lark, K.A.; Barker, D.R. Modeling of dynamic material behavior in hot deformation: Forging of Ti-6242. *Metall. Trans. A* **1984**, *15*, 1883–1892. [[CrossRef](#)]
39. Prasad, Y.V.R.K. Author's reply: Dynamic materials model: Basis and principles. *Metall. Mater. Trans. A* **1996**, *27*, 235–236. [[CrossRef](#)]
40. Prasad, Y.V.R.K.; Seshacharyulu, T. Modelling of hot deformation for microstructural control. *Int. Mater. Rev.* **1998**, *43*, 243–258. [[CrossRef](#)]
41. Seshacharyulu, T.; Medeiros, S.C.; Frazier, W.G.; Prasad, Y.V.R.K. Hot working of commercial Ti-6Al-4V with an equiaxed α - β microstructure: Materials modeling considerations. *Mater. Sci. Eng. A* **2000**, *284*, 184–194. [[CrossRef](#)]
42. Peng, X.N.; Guo, H.Z.; Shi, Z.F.; Qin, C.; Zhao, Z.L.; Yao, Z.K. Study on the hot deformation behavior of TC4-DT alloy with equiaxed α + β starting structure based on processing map. *Mater. Sci. Eng. A* **2014**, *605*, 80–88. [[CrossRef](#)]
43. Sivakesavam, O.; Rao, I.S.; Prasad, Y.V.R.K. Processing map for hot working of as cast magnesium. *Mater. Sci. Technol.* **1993**, *9*, 805–810.
44. Srinivasan, N.; Prasad, Y.V.R.K. Characterisation of dynamic recrystallisation in nickel using processing map for hot deformation. *Mater. Sci. Technol.* **1992**, *8*, 206–212. [[CrossRef](#)]
45. Ravichandran, N.; Prasad, Y.V.R.K. Dynamic recrystallization during hot deformation of aluminum: A study using processing maps. *Metall. Trans.* **1991**, *22*, 2339–2348. [[CrossRef](#)]
46. Tan, Y.B.; Ma, Y.H.; Zhao, F. Hot deformation behavior and constitutive modeling of fine grained Inconel 718 superalloy. *J. Alloy. Compd.* **2018**, *741*, 85–96. [[CrossRef](#)]
47. Wan, Z.P.; Hu, L.X.; Sun, Y.; Wang, T.; Li, Z. Hot deformation behavior and processing workability of a Ni-based alloy. *J. Alloy. Compd.* **2018**, *769*, 367–375. [[CrossRef](#)]
48. Li, H.Z.; Wang, H.J.; Li, Z.; Liu, C.M.; Liu, H.T. Flow behavior and processing map of as-cast Mg-10Gd-4.8 Y-2Zn-0.6 Zr alloy. *Mater. Sci. Eng. A* **2010**, *528*, 154–160. [[CrossRef](#)]
49. Lu, S.Q.; Li, X.; Wang, K.L.; Dong, X.J.; Fu, M.W. High temperature deformation behavior and optimization of hot compression process parameters in TC11 titanium alloy with coarse lamellar original microstructure. *Trans. Nonferrous Met. Soc. China* **2013**, *23*, 353–360. [[CrossRef](#)]

